Mon. Not. R. Astron. Soc. **366,** 945–952 (2006) doi:10.1111/j.1365-2966.2005.09743.x

Observational constraints on the radio and γ-ray emission regions of PSR B1055−52

H. G. Wang,[1⋆] G. J. Qiao,[2⋆] R. X. Xu[2⋆] and Y. Liu[1⋆]

[1]*Center for Astrophysics, Guangzhou University, Guangzhou 510400, China*
[2]*Department of Astronomy, Peking University, Beijing 100871, China*

Accepted 2005 October 14. Received 2005 October 13; in original form 2005 February 17

ABSTRACT

Observational constraints on the radio and γ-ray emission regions of PSR B1055−52 seen through our line of sight are presented by analysing the position angle curves of radio linear polarization and fitting the observed pulse widths of radio and γ-ray pulses and the phase offsets between them. Aberration, retardation and magnetic field sweep back effects that can cause additional phase offset between the emissions from different locations are taken into account. The following conclusions are obtained. (i) The radio main pulse and γ-ray pulses are emitted from the same pole, while the radio interpulse is emitted from the opposite pole. (ii) The interpulse emission region locates on the open field lines much closer to the magnetic axis than those of the main pulse, and the emission altitudes are higher than those of the main pulse. (iii) At each pole, there are probably two groups of field lines where radio emission is generated, of which the outer one consists of open field lines near (or including) the last open field lines and the inner one consists of open field lines from very near the magnetic pole to approximately the midway between the magnetic axis and the last open field lines. (iv) The γ-ray pulse comes from inner open field lines rather than from the last open field lines, and the emission altitudes are beyond the null charge surface.

Key words: radiation mechanisms: non-thermal – pulsars: individual: PSR B1055−52.

1 INTRODUCTION

More and more high-energy observational data are accumulated for pulsars, but the high-energy emission mechanisms and regions are still a matter of debate. In the literatures, the polar cap model (Harding 1981; Daugherty & Harding 1996), the outer gap model (Cheng, Ho & Ruderman 1986a,b; Cheng, Ruderman & Zhang 2000), the two-pole caustic model (Dyks & Rudak 2003), the slot gap model (Muslimov & Harding 2004) and the annular gap model (Qiao et al. 2004) have been proposed to account for the γ-ray emission of pulsars, in which the suggested emission locations are different from each other. Therefore, it is necessary to make observational constraints on the emission locations to test those theories. PSR B1055−52, thanks to its unique emission properties revealed by resourceful multiband observations, is a good one to perform such studies.

At radio frequencies, PSR B1055−52 has a strong interpulse (IP) follows the main pulse (MP) by a phase offset of 155° (McCulloch et al. 1976; Lyne & Manchester 1988, hereafter LM88). The variations of the position angle (hereafter PA) of linear polarization across the MP and IP both follow 'S' shapes, but their maximum rates of PA swing, $(\mathrm{d}\psi/\mathrm{d}\Phi)_{\max}$, differ very much, which are approximately 1.6 deg deg^{-1} at the MP and 7.0 deg deg^{-1} at the IP. The linear polarized percentage of the trailing component is much lower than that of the leading one at the IP as well as that of the MP (LM88).

The γ-ray light curve of PSR B1055−52 shows double peaks with a separation of ∼80° (defined as the width between the central phases of the peaks). Multiband observations reveal that the central phase of the radio MP lags the trailing γ-ray peak (hereafter TGP) by ∼20° (Thompson et al. 1999; see Fig. 1). This property is completely different from that of the Crab pulsar, which shows that the radio MP and IPs are well aligned with the two γ-ray peaks. It is also different from the Vela and Vela-like pulsars (PSR B1706−44, B1951+32 and B1509−58), of which the leading γ-ray peak (hereafter LGP) usually lags the radio pulse by an offset of less than 90°.

In this paper, we focus on constraining the emission regions of PSR B1055−52 seen through the line of sight (LOS) via a geometrical method. The main idea is as follows. Supposing that for a pulsar with a fixed inclination angle, the γ-ray photons are emitted from a group of open field lines and a range of altitudes, thus form a γ-ray emission beam, and so do the radio MP and IP emission beams. When the LOS sweeps across the beams, we see the radio and γ-ray pulses (GPs). The observed pulse widths are related to

⋆E-mail: wanghg@gzhu.edu.cn (HGW); gjn@pku.edu.cn (GJQ); r.x.xu@pku.edu.cn (RXX); pinux@pku.org.cn (YL)

the geometry of the emission regions as well as the inclination angle α and the viewing angle ζ (between the LOS and the rotation axis). The phase offset between the pulses is attributed to the original phase offset due to the separation of the field lines, where the pulses originate and the additional offset caused by aberration, retardation and magnetic field sweep back (hereafter MSB) effects. Therefore, in principle one can constrain the emission regions by fitting the observed pulse widths and the phase offsets, but first of all some general geometrical parameters (i.e. from which poles the MP, the IP and the GP are viewed and the values of α and ζ) must be determined definitely, then one could make definite constraints. Usually, α and ζ can be obtained by fitting the PAs of linear polarization (LM88), hereafter we adopt the best-fitting values of $\alpha = 74.^{\circ}7$ and $\zeta = 113.^{\circ}4$ for B1055−52 given by LM88.[1] The paper is organized as follows. In Section 2, the polar origin of the radio and GPs is determined; in Section 3, the geometrical method is described first and then the emission regions and the geometry of radio and γ-ray emission beams are constrained. Conclusions and discussion are presented in Section 4.

2 THE ORIGIN: ONE POLE VERSUS TWO POLE

In this section, we will show that the radio MP and the GP should come from the same pole, while the radio IP should come from the opposite pole. For convenience, we define the pole where the radio MP/GPs are emitted as pole 1 (P1), and that where the IP is emitted as pole 2 (P2).

2.1 The origin of radio MP and IP

The two-pole origin of the radio MP and the IP has been suggested by LM88.[2] From a different respect, we reanalyse the radio PA curves and confirm their suggestion. Briefly to say, under the frame of the rotating vector model (hereafter RVM; Radhakrishnan & Cooke 1969, hereafter RC69) that is widely adopted to explain the PA curves of pulsars, the observed phase separation between the PA curves of the MP and IP and the positive maximum derivative of PA curves of both the pulses cannot be reproduced if the radio MP and IP are observed from the same pole. In contrast, the observed PA curves can be well fitted by the RVM model under the assumption that the MP and the IP come from opposite poles.

In the RVM model, the PA curve is suggested to reflect the variation of orientation of the magnetic field lines with respect to the Ω–μ plane (the plane containing the rotational and the magnetic axes), which can be described as (RC69)

$$\tan(\Psi - \Psi_0) = \frac{\sin\alpha \sin\Phi}{\sin\zeta\cos\alpha - \cos\zeta\sin\alpha\cos\Phi}, \quad (1)$$

[1] In the present paper, ζ is defined as $\alpha + \beta_{\rm MP}$, where $\beta_{\rm MP}$ is the impact angle of the MP. LM88 gave a result of $\beta_{\rm MP} = 38.^{\circ}7$ and $\alpha = 74.7$, thus the viewing angle is $113.^{\circ}4$. In LM88, ζ is defined as $\alpha + \beta_{\rm IP}$ for B1055−52. They obtained $\beta_{\rm IP} = -7.^{\circ}9$, then $\zeta = 66.^{\circ}6$. There is a relation between our ζ and theirs, i.e. $\zeta_{\rm our} + \zeta_{\rm LM88} = 180^{\circ}$. Despite such difference, the PA curves with these two definitions are the same.

[2] Their suggestion is based on two major reasons. (i) The low linear polarization in the trailing component of the IP and the inflection of the PA curve of this component make the authors believe that the low-polarized component is a core or inner component, while the trailing conal component is missing, thereby the 'true' separation between the MP and the IP should be $\sim 180^{\circ}$. (ii) The optimum inclination angle $\alpha = 74.^{\circ}7$ obtained by fitting the PA curves indicates that this pulsar is nearly an orthogonal rotator.

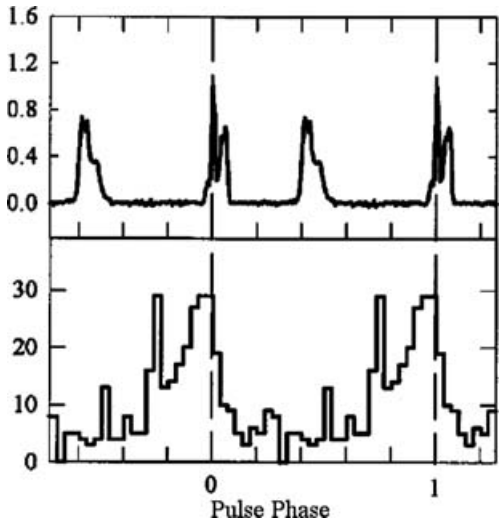

Figure 1. The phase-aligned radio profile and γ-ray light curve of B1055−52 (Thompson et al. 1999). The phase of leading peak of MP is chosen as a reference and is shown by a vertical dashed line.

where Ψ is the PA, Ψ_0 represents the PA of the magnetic field lines on the Ω–μ plane and Φ is the longitude counted along the direction of LOS and defined as zero on the Ω–μ plane. Examples of model PA curve are shown in Fig. 2 with ($\alpha = 74.^{\circ}7, \zeta = 113.^{\circ}4$) and ($\alpha = 10^{\circ}, \zeta = 11.^{\circ}5$).

First, let us assume that the radio MP and IP are observed from the same magnetic pole. In the simplest case, we assume that both of the pulses originate from the magnetic field lines that are symmetric to the Ω–μ plane. From fig. 8 of LM88, the phase separation between the centres of PA curves (where the maximum derivatives are reached) of MP and IP is approximately 170°,[3] then the phases of centres of PA curves are -85° for the MP and 85° for the IP, respectively. The large phase separation suggests a nearly aligned rotator wherein the MP and IP may come from the same emission cone. Can the PA curves be explained in this situation? The main feature of the PA curves is that the maximum derivatives are approximately 1.6 deg deg^{-1} in the MP and 7.0 deg deg^{-1} in the IP. We developed a code to find in which region of (α, ζ) the observed maximum derivatives can be reached at the phases $\Phi = \pm 85^{\circ}$. Given a fixed value of the derivative $d\Psi/d\Phi$ and with $\Phi = 85^{\circ}$, the code calculates $d\Psi/d\Phi$ for each group of (α, ζ) and searches all the (α, ζ) that produce the given derivative and then plots them in a contour map. Fig. 3 shows the contour lines for $d\Psi/d\Phi$ from -0.20 to 0.99 deg deg^{-1}, respectively. Numerical calculation finds that no PA derivatives greater than 1.0 could be reached within the whole ($\alpha - \zeta$) domain [$\alpha \in [0, 90^{\circ}]$, $\zeta \in [0, 180^{\circ})$], as shown in Fig. 3. Neither the observed maximum derivative of the MP nor that of the IP can be reproduced.

From the different slope rates of PA curves, one may conjecture that the emission region of the MP and the IP may be asymmetric to the Ω–μ plane. However, we failed to find any solution of α and ζ to fit the observed slope rates for this situation. For the PA curves with small and moderate inclination angles, e.g. $\alpha = 10^{\circ}$ (see Fig. 2 for an example) and $\alpha = 50^{\circ}$, although the maximum

[3] The maximum derivative of PA curve occurs nearly at the centre of the MP but nearly at the last PA data point in the IP. Therefore, the separation between the centres of PA curves is different from that between the centres of the intensity profiles.

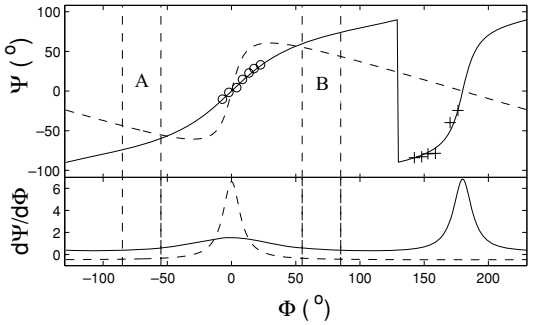

Figure 2. The PA curve (upper panel) and the derivative $d\Psi/d\Phi$ (lower panel) are presented for $\alpha = 74.^{\circ}7$ and $\zeta = 113.^{\circ}4$ by solid curves. In the case of two-pole origin, the MP and IP concentrate on longitudes around $\Phi \sim 0$ and $\Phi \sim 180^{\circ}$, respectively. The observed PA data are adopted from fig. 8 of LM88 (the circles for the MP and the crosses for the IP), but shift 90° down and 123° left to be coincident with the definition of $\Psi_0 = 0$ and $\Phi_\circ = 0$ in RVM. In the case of single-pole origin, the MP and IP should be symmetric to $\Phi = 0$, which are represented by regions A and B, respectively. Certainly, the PA curves in A and B cannot fit the observed data. In addition, the PA swing and derivative are presented for $\alpha = 10^{\circ}$ and $\zeta = 11.^{\circ}5$ by dashed curves to show as an example that the observed data cannot be fit with a small inclination angle.

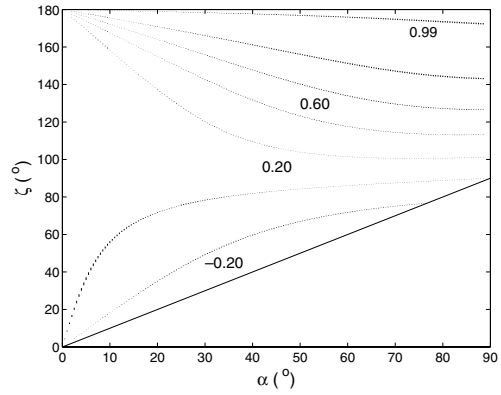

Figure 3. The contour lines for the PA derivative at ($\Phi = \pm 85^{\circ}$) in the case of single-pole origin (see the text). The contours are calculated with RVM model for $d\Psi/d\Phi = -0.20$–0.80 deg deg^{-1} with a step of 0.20 and additionally $d\Psi/d\Phi = 0.99$ deg deg^{-1} (dotted curves). The solid line is $\zeta = \alpha$. No PA derivatives greater than 1.0 are reached within the $\zeta > \alpha$ domain. The calculation is not performed in the region $\zeta < \alpha$ where the PA derivatives are all negative within the whole pulse phase.

derivative can reach the value as large as that of the IP, the total phase range of positive slope rates is much smaller than 170°. For large inclination angles and suitable viewing angles ($\zeta > 180 - \alpha$), e.g. $\alpha = 74.^{\circ}7$ and $\zeta = 113.^{\circ}4$, the PA curves can be fitted, which requires that our LOS sweeps across the lower edge of the emission beam to produce the IP (with longitudes around $\Phi \sim 0^{\circ}$ and a larger maximum PA derivative) and then the upper edge of the same beam on the opposite side to produce the MP (with longitudes around $\Phi \sim 170^{\circ}$ and a less maximum PA derivative). However, that would arise a serious problem, because the beam radius ρ on the upper edge would be $\rho \simeq \zeta + \alpha \sim 180^{\circ}$, which is so large that the radio emission has to come from regions very near the light cylinder. It seems implausible because many authors have found that radio emission region is close to the polar cap rather than near the light cylinder (Cordes 1978; Smirnova & Shishov 1989; Phillips 1992; Rankin 1993; Wu, Huang & Xu 2002). From the above analysis, the possibility that both the radio MP and the IP are observed from the same pole can be ruled out.

In the case of two-pole origin, the observed PA data can be naturally explained and well fitted by the RVM, as shown in Fig. 2, where the observed data and best-fitting PA curve are adopted from fig. 8 of LM88, but all the PAs subtract 90° and the longitudes subtract 123° to be coincident with the conventional definition of $\Psi_0 = 0$ and $\Phi_0 = 0$ in RVM. The best-fitting curve is reproduced with $\alpha = 74.^{\circ}7$ and $\zeta = 113.^{\circ}4$. Note that the fit is performed in standard RVM, i.e. the aberration, retardation and MSB effects that cause the pulse phase and PA change are not involved. It was found that these effects may shift the PA curves in both the pulse phase and the PA value, however, the change of the slope rates of PA curve is minor (Blaskiewicz, Cordes & Wasserman 1991; Hibschman & Arons 2001). Since $\alpha = 74.^{\circ}7$ and $\zeta = 113.^{\circ}4$ best fit the slope rates of the PA curves, especially the maximum rates in standard RVM, we believe that such values of α and ζ should still hold viable when those effects are considered.

2.2 The origin of GP

The GP emission should be emitted from P1, otherwise the observed phase offsets between the radio and GPs cannot be naturally explained. The demonstration is as follows. (i) The LGP should not come from P2. Here, the observed phase offsets we concern are: the LGP lags the MP by $\sim 260^{\circ}$ and the IP lags the MP by $\sim 155^{\circ}$. Supposing that the LGP comes from P2, subtracting the original offset of 180° between P1 and P2, the additional offsets that the LGP lags the MP and the IP lags the MP are $\sim 80^{\circ}$ and $\sim -25^{\circ}$, respectively. The additional offset is caused by the aberration and retardation effects which make the emission from higher altitude arrive earlier than that from lower altitudes. In addition, there is a competing MSB effect and it depends on the actual emission altitude which effect dominates (see Section 3 for details). Then, the IP emission heights should be higher than those of the MP, and the MP emission heights should be higher than those of the γ-rays. If we only consider the aberration and retardation effects, the emission heights of the radio MP and IP have to be at least $0.7r_{\rm c}$ and $0.95r_{\rm c}$ even when the γ-ray heights are nearly zero, where $r_{\rm c}$ is the radius of the light cylinder. Again, the radio altitudes are implausibly too high. When taking into account all the three effects, we failed to find a solution for the IP within the light cylinder. (ii) The TGP should not come from P2. Here, we concern the observed offset of $\sim 180^{\circ}$ between the TGP and the IP. If the TGP comes from P2, the same pole as the IP, the additional phase offsets would be $\sim 180^{\circ}$. As we estimated, even a difference of $0.95r_{\rm c}$ of their altitudes can only generate additional offsets less than $\sim 70^{\circ}$, much smaller than 180°, therefore there is little possibility that the TGP comes from P2. (iii) If the LGP and TGP come from P1, reasonable solution of the emission altitudes can be obtained (see Table 1). As to the bridge emission, it is natural that they have the same origin as the peaks.

3 CONSTRAINTS ON THE RADIO AND γ-RAY EMISSION REGIONS

Taking the polar origin of the radio and GPs determined above and the values of α and ζ given by LM88, we are to constrain the γ-ray emission regions by fitting the observed pulse widths and phase offsets. The geometrical method is described first and then the results are presented.

Table 1. Parameters for the radio and γ-ray emission. '-C' and '-L' stand for the central and leading positions of the MP, the IP or the GP. The apparent pulse widths of MP, IP and GPs are approximately 30°, 48° and 80°, respectively, which are used to determine observed additional phase offset $\Delta\Phi_{\rm add,o}$. The symbol '†' indicates that the trailing conal component of the IP is assumed to be missing, in this case the total width of IP is assumed to be 72°, i.e. 1.5 times the observed IP width. The symbol '‡' indicates no component of the IP is missing. Columns 3 and 4 are the observed phase offsets used in the constraining process. Columns 5–8 are the constrained results with method A. Columns 9 and 10 are intermediate parameters. Columns 11 and 12 are results with method B. See Section 3.2 for descriptions of these parameters.

Emission points	Pole	$\Delta\Phi_{\rm app}$ (°)	$\Delta\Phi_{\rm add,o}$ (°)	φ (°)	η (°)	$r/r_{\rm c}$	$r/r_{\rm ncs}$	$r_{\rm e}/r_{\rm c}$	$r_{\rm ncs}/r_{\rm c}$	η^*	$r^*/r_{\rm c}$
MP-C	1	0	0	0	1.0	0.34	5.8	1.87	0.059	1.0	0.34
MP-L	1	15	0	21.1	1.0	0.35	5.7	1.71	0.061	1.0	0.35
IP-C†	2	170	−10	0	0.20	0.43	–	48.6	–	0.19	0.46
IP-L†	2	134	−10	70.7	0.60	0.46	–	2.94	–	0.57	0.49
IP-C‡	2	170	−10	0	0.20	0.43	–	48.6	–	0.19	0.46
IP-L‡	2	134	−22	66.6	0.39	0.55	–	7.28	–	0.33	0.74
GP-C	1	−30	−30	0	0.77	0.59	5.4	3.19	0.11	0.63	0.86
GP-L	1	−100	−60	46.0	0.73	0.83	5.2	2.47	0.16	–	–

3.1 The geometrical method

The main idea of this method is to fit the observed pulse width by using geometrical relations and fit the phase offsets by taking into account the aberration, retardation and MSB effects. The basic assumptions are: (i) the magnetic field is dipolar and (ii) all the emission regions are symmetrical to the Ω–μ plane. Since the observed offsets been fitted are those between the MP and the IP/GP, the emission region of the MP must be determined definitely in the beginning so that it could be used as a fixed reference to calculate the model offsets and compare them with the observed offsets. Therefore, we make an additional assumption that the MP is emitted from the last open field lines for simplicity. As will be discussed at the end of this section, this assumption does not change the conclusion.

The key parameters of the emission regions that we want to know are the emission altitude r, the azimuthal angle φ between the magnetic field plane and the Ω–μ plane and a factor η defined as $\eta = \theta_\varphi/\theta_{\varphi,0}$, where θ_φ is the polar angle of the foot point of an open field line on polar cap surface and subscript '0' stands for the last open field lines, r is counted from the stellar centre to the emission point, φ is counted anticlockwise when viewing downwards from each pole, $\varphi = 0$ is defined when the field lines are located on Ω–μ plane and meanwhile are curved towards the equatorial plane. The parameters φ and η denote the open field lines where photons are emitted. η varies from 0 (representing the magnetic axis) to 1 (representing the last open field lines); a smaller value of η means that the field line is more inner or closer to the magnetic axis.

For the emission regions symmetric to Ω–μ plane, two positions are enough to represent the emission region viewed by the LOS, of which one is the emission point at the field line on the Ω–μ plane (with $\varphi = 0$ when $\zeta > \alpha$, hereafter called the central position, marked with '-C' in Table 1), the other is the emission point at nearly the outmost leading field line with respect to the Ω–μ plane that corresponds to the leading edge of the radio/GP (with $\varphi \neq 0$, hereafter called the leading position and marked with '-L'). Our aim is to derive r, φ and η for the central and leading positions. In a dipolar magnetic field, when the emission comes from the field lines with the same η, e.g. the last open field lines with $\eta = 1$, the radius of the central position is the lowest, while that of the leading position is the highest. For the reason of symmetry, the parameters of the trailing point should have the same values as those of the leading position.

The procedure of this method follows two steps, first φ is determined for the central and leading emission positions and then r and η are constrained.

In the first step, φ can be figured out for the leading positions from the observed pulse width W with the relations given by the beaming geometry model (Gil, Gronkowski & Rudnicki 1984; LM88), i.e.

$$\sin^2\frac{\theta_\mu}{2} = \sin^2\frac{W}{2}\sin\alpha\sin\zeta + \sin^2\frac{\zeta-\alpha}{2}, \tag{2}$$

$$\tan\frac{\pi-\varphi}{2} = \sqrt{\frac{\sin(p-\alpha)\sin(p-\theta_\mu)}{\sin(p-\zeta)\sin p}}, \tag{3}$$

where θ_μ is the beaming angle between the photon direction and the magnetic axis and $p = (\alpha + \zeta + \theta_\mu)/2$. In this paper, radio pulse width is defined as the separation between the leading and trailing edges of pulse profile where their intensities are 20 per cent of the leading and trailing peaks, respectively, which is called 20 per cent width hereafter. The GP width is the phase separation between the centres of the bins of leading and trailing peaks. The pulse widths of MP, IP and GPs are approximately 30°, 48° and 80°, respectively. For the central positions, just let $W = 0$ to calculate φ.

In the second step, the main relations used to calculate r and η are based on the geometry of the dipolar field

$$\theta = \tan^{-1}\left(\frac{-3 \pm \sqrt{9 + 8\tan^2\theta_\mu}}{2\tan\theta_\mu}\right), \tag{4}$$

$$r = \eta^{-2} r_{\rm e,0}\sin^2\theta, \tag{5}$$

where θ is the polar angle of an emission point, signs '+' and '−' apply to $\theta_\mu \in [0, \pi/2)$ and $\theta_\mu \in (\pi/2, \pi]$, respectively, $r_{\rm e,0}$ is the maximum radius of the last open field line, which is a function of φ and α and can be numerically solved by tracing the point where the last open field line is tangent to the light cylinder. Obviously, η must be given to determine r. For the MP, we assume $\eta = 1$, for the other pulses, r and η are simultaneous output by fitting the observed phase offsets. Such processes are as follows: (i) given a set of values of η, a set of r is obtained with equation (5); (ii) calculate the additional phase offsets between γ-ray (IP) central/leading positions and the central position of MP by involving three kinds of effects; (iii) compare them with the observed additional phase offsets and select appropriate solutions of η and r that can account for

observational data. The values of φ determined in the first step are used in this step.

Finally, three effects that cause additional phase offsets are introduced below.

(i) Aberration effect: because the relativistic charges that emit photons are confined to move along the magnetic field lines, they have a corotation velocity, thereby the photon direction shifts an angle towards the corotation direction with respect to the original photon direction (parallel to the magnetic field) in the corotation rest frame. This effect causes photons arrive earlier. Let ϑ denote the angle between the photon direction and the corotation velocity in the observer's frame and ϑ' in the corotation rest frame, one has

$$\tan\vartheta = \sin\vartheta'/[\gamma(\cos\vartheta' + r\sin\delta/r_{\rm c})], \quad (6)$$

where δ is the angle between the radius r and the Ω-axis, $\gamma = [1-(r\sin\delta/r_{\rm c})^2]^{-1/2}$ (see Appendix for the geometrical relations of δ and ϑ' and Fig. A1 therein). Then, the phase shift reads $\delta\Phi_{\rm abe} \simeq \vartheta - \vartheta'$.

(ii) Retardation effect: comparing with those photons travelling from the stellar centre, the photons emitted from radius r will arrive earlier by a time interval $\delta t = r\cos\sigma/c$, thus giving a phase shift $\delta\Phi_{\rm ret} = \Omega\delta t = r\cos\sigma/r_{\rm c}$, where c is the light velocity, Ω is the angular velocity of the star and σ is the angle between the radius r and the photon direction. If we neglect the shift of photon direction caused by aberration in order to simplify the calculation, there is a simple relation $\sigma = \theta_\mu - \theta$.

(iii) Shitov (1983) first noted that the magnetic-dipole radiation wave generated by a rotating neutron star exerts a torque on the magnetic field and consequently causes the field lines to sweep back. As he estimated, the direction of the distorted magnetic field deflects from the direction of the pure dipole by an angle

$$\delta\Phi_{\rm msb} \sim 1.2(r/r_{\rm c})^3\sin^2\alpha. \quad (7)$$

In contrast to aberration and retardation effects, this effect makes the emission from higher altitudes arrive later than that from lower altitudes. It is a higher order effect with respect to the aberration and retardation effects, so later authors used to neglect the sweep back effect when studying the radio PA curves or profiles where the radio emission altitudes are well within the light cylinder (e.g. Blaskiewicz et al. 1991; Hibschman & Arons 2001). However, at high altitudes the phase shift due to this effect can be comparable or even larger than that caused by aberration or retardation effect, thus it should be taken into account when calculating the emission altitudes.

For a fixed emission point, the longitude of the emission should be modified by considering the above three effects. However, equation (7) is a rough estimation for MSB effect and barely applicable to a vacuum magnetosphere. Since it is not so precise as the estimations of aberration and retardation effects, we perform the constraining in two ways, of which one only considers the aberration and retardation effects (hereafter method A) and the other includes all three kinds of effects (hereafter method B). In fact, the results show that method B is not successful to find solutions when emission height is very high, indicating better estimation for MSB effect is needed.

In method A, the additional phase offset between a γ-ray or IP emission point with respect to the central point of MP is $\Delta\Phi_{\rm add} = (\delta\Phi_{\rm abr}+\delta\Phi_{\rm ret}) - (\delta\Phi_{\rm abr}+\delta\Phi_{\rm ret})_{\rm MP,C}$. It is this phase offset that will be calculated and compared with the observational data ($\Delta\Phi_{\rm add,o}$, see below) in the constraining process. In method B, the definition of additional phase offset changes to $\Delta\Phi_{\rm add} = (\delta\Phi_{\rm abr}+\delta\Phi_{\rm ret}-\delta\Phi_{\rm msb}) - (\delta\Phi_{\rm abr}+\delta\Phi_{\rm ret}-\delta\Phi_{\rm msb})_{\rm MP,C}$.

3.2 The results

The results for the central and leading positions are presented in Table 1, where 'MP', 'IP' and 'GP' denote the radio MP, IP and GP, respectively. First of all, the information that is used in the constraining process is given from Columns 2–4. Column 2 is the pole where the emission comes from. Column 3 is the apparent phase offset $\Delta\Phi_{\rm app}$ between a certain emission position and the central position of MP. The longitudes of central positions of MP and IP are measured at the centres of PA curves (where maximum derivatives are reached).[4] Since there are no PA information for the GP, $\Delta\Phi_{\rm app}$ of γ-ray central position is first measured from the separation between the centres of GP and PA curve of MP, which is -60°, and then adjusted to -30° by hand by considering the influence of aberration, retardation and MSB effects. The leading positions of MP and IP are designated to be corresponding to the points at the leading edge of pulse profiles where the intensities are 20 per cent of the leading peaks. The γ-ray leading position are designated as the centre of the bin of LGP. From $\Delta\Phi_{\rm app}$ and pulse widths, the observed additional phase offsets $\Delta\Phi_{\rm add,o}$ are determined following the principle $\Delta\Phi_{\rm add,o} = \Delta\Phi_{\rm app} - \Delta\Phi_{\rm pp} - W/2$ ($W = 0$ for central points), where $\Delta\Phi_{\rm pp}$ is the offset from pole to pole (0 for the same pole and 180° for opposite poles). The results are listed in Column 4. The symbol '†' indicates that the trailing conal component of the IP is assumed to be missing, as suggested by LM88. In this case, the total width of IP is assumed to be $72^{\rm o}$, i.e. 1.5 times the observed width of 48°. The symbol '‡' indicates that the total IP is assumed to come from a full radio beam and no component is missing.

With method A, the constrained φ, η and r in unit of $r_{\rm c}$ and $r_{\rm ncs}$ are listed in Columns 5–8, where $r_{\rm ncs}$ is the radius of the null charge surface wherein $\mathbf{\Omega}\cdot\mathbf{B} = 0$ is satisfied (Goldreich & Julian 1969). The intermediate parameters $r_{\rm e}$ (the maximum radius of an open field line in the case of pure dipolar magnetic field) and $r_{\rm ncs}$ are also shown in Columns 9 and 10. As a comparison, the results of η and r with method B are listed in Columns 11 and 12, marked with a symbol '*'. It shows that the field line becomes more inner and the emission altitude becomes higher than those obtained with method A. In addition, there are no solutions for the γ-ray leading position. However, generally there is no essential difference between the results obtained with these two methods. In the following, we mainly summarize and analyse the results of method A. Then, the results of method B will be explained a little more, mainly on the role of the MSB effect.

The results of model A show a clear picture that the IP and the GP come from much inner field lines and higher altitudes than those of the MP. The details of the emission regions viewed by the LOS are as follows. (i) The MP emission region spans the last open field lines with φ from -21° to 21°. The emission heights are from 0.34 to $0.35r_{\rm c}$, varying only a little so that the aberration and retardation effects are negligible. (ii) For the IP, no matter one assumes that the IP is partially missing or not missing, the results show the same picture, i.e. the emission comes from much inner open field lines with $\eta < \sim 0.6$ and from $\varphi \sim -70^\circ$ to $\sim 70^\circ$, meanwhile the emission

[4] Due to aberration and retardation effects, the longitude of emission from central position will be shifted to trailing part of pulse profile when the emission height of central position is the lowest in the emission region. It is hard to tell the exact longitude of central position from purely the pulse profile. However, the maximum derivative of PA curve still occurs at or very near the central position even considering the three effects. Therefore, it is more reliable to choose the centres of PA curves to represent central positions than to choose the apparent centres of pulse profiles.

altitudes are higher than those of the MP. (iii) The γ-ray emission region comes from inner open field lines with $0.7 < \eta < 0.8$ and spans from $\varphi \simeq -46^\circ$ to 46°. The emission radius is about 0.6–$0.8r_c$, approximately five times the radius of the null charge surface at each open field line. (iv) Intuitively, the emission patterns should be the same on two poles. Combining with the results of the MP and IP, it suggests that strong radio emission concentrates on at least two groups of open field lines: the outer are the (or very near the) last open field lines and the inner are the field lines with $\eta < \sim 0.6$. (If one adopts that the trailing conal component of IP is missing, there might be an additional innermost group of field lines with $\eta \sim 0.2$, where the core component is emitted). This configuration is shown in Fig. 5(a), where the central positions of the three emission regions are plotted in the Ω–μ plane.

Why must the IP and GP come from inner field lines and higher altitudes than the MP? Note that abberation and retardation effects make emission from higher altitudes arrive earlier in longitude, then negative additional phase offsets of IP and GP require that their emissions come from higher altitudes. However, because the LOS sweeps the IP region more closely to the pole, the IP would come from lower altitudes at the last open field lines, thus inner field lines are needed to increase the altitudes. For the GP, inner field lines are also needed to increase the altitudes significantly. From the above analysis, it is easy to see that the basic picture does not change if one assumes that the MP originates from inner field lines.

Besides the basic picture mention above, the results show two particular properties. The first is the asymmetry of the MP and γ-ray emission beams, the second is the high radio emission altitudes. (i) The radio and γ-ray emission beams on P1 and P2 are schematically shown in Figs 5(b) and (c) together with the LOS. The γ-ray and radio MP beams (MPBs) are plotted as half rings to avoid being seen from P2 (this is an extreme case, there may be some other possibilities, but the asymmetry is still required in those situations). It suggests that the γ-ray emission and the MP emission must be severely asymmetric between the lower (close to the equator) and the upper (close to the rotational axis) parts of the magnetosphere. (ii) The emission radius of the MP and IP that we observed are all greater than $0.3r_{\rm rc}$, i.e. $\sim$2820 km, which is higher than the radio emission heights of many other pulsars obtained by previous authors (e.g. Rankin 1993, usually a few hundred kilometres for normal pulsars).

Finally, let us focus a bit more on the results of method B. Qualitatively, the altitudes should increase when considering the sweep back effect because this effect partially cancels the influence of abberation and retardation effects. As an example, the plot of additional phase offset versus emission height that is used to constrain the height of γ-ray central position is show in Fig. 4. The contributions from aberration, retardation and MSB effects are plotted as green, red and blue curves, respectively; the sum of aberration and retardation effects are shown as a dashed black curve; the sum of all the three effect are plotted as a solid black curve. The additional phase offset derived from observation, $\Delta\Phi_{\rm add,o} = -30$, is shown as a dashed blue line. The cross points of the blue line and two black curves determine the solutions of r for methods A and B. Obviously, when the MSB effect is considered, the absolute value of $\Delta\Phi_{\rm add}$ increases with r (solid black curve) more slowly than it does when the effect is not included (dashed black curve), therefore, higher altitude is obtained with method B.

Since the MSB effect greatly reduces the absolute value of additional phase offset at high altitudes, e.g. $r > 0.6r_c$, it is the main reason for non-solution of the γ-ray leading position. If the real influence of MSB effect is less than that estimated by Shitov's equation, it would be beneficial to finding a solution.

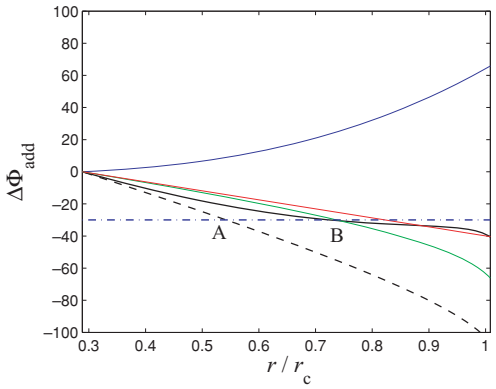

Figure 4. The plot of additional phase offset $\Delta\Phi_{\rm add}$ versus emission height r in unit of radius of light cylinder r_c for the γ-ray central position. The green, red and blue curves represent the contributions from aberration, retardation and MSB effects, respectively. The dashed black curve is the sum of aberration and retardation effects. The solid black curve is the sum of all the three effects. The additional phase offset derived from observation, $\Delta\Phi_{\rm add,o} = -30$, is shown as a dot–dashed blue line. The intersection points of the blue line and two black curves, marked with 'A' and 'B', determine the solutions of r for methods A and B, respectively.

4 CONCLUSION AND DISCUSSION

PSR B1055−52 shows unique multiband properties among all the known seven γ-ray pulsars. In this paper, we make constraints on both the radio and the γ-ray emission regions viewed by the LOS. By considering the aberration, retardation and MSB effects that influence the longitudes of emission, we fit the observed pulse widths and phase offsets between radio MP, IP and GP. The conclusions are as follows.

(i) The radio MP and GPs are emitted from the same pole, while the radio IP is emitted from the opposite pole.

(ii) The radio IP and the GP come from much inner field lines and higher altitudes than the radio MP. The γ-ray emission altitudes viewed by our LOS are beyond the null charge surface.

(iii) At each pole, there are probably two groups of field lines where radio emission is generated. The outer one consists of open field lines near (or including) the last open field lines, and the inner one consists of open field lines from very near the magnetic pole to approximately the midway between the magnetic axis and the last open field lines.

In this paper, we assume that the γ-ray and radio emission regions are symmetric about the Ω–μ plane. In fact, the GP does not seem to be so symmetric as that of the Crab or Vela pulsar. Instead, the leading peak is very narrow and the trailing component is much wider. We cannot exclude the possibility that asymmetry happens to emission regions. If this assumption is relaxed, the configuration of the γ-ray and radio pulses would be arbitrary and the computations would be difficult to perform.

The conclusion that the MP and IP originate from two opposite poles is based on the distinctive slope rates of their PA curves. It should be noted that the inflection of the PA curve occurs at the trailing component (only two points of data are observed there), where the linear polarization is much lower than that of the leading one. Are those two points crucial to determine the double-pole origin of MP and IP? Without those two points, the maximum slope rate of PA of the IP drops to about 0.3, while that of the MP remains to be 1.6. The demonstration performed in Section 2 still holds valid.

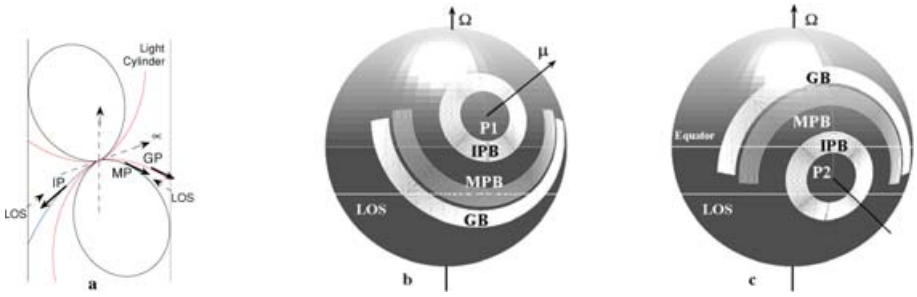

Figure 5. (a) The 2D diagram for the observed central positions of the MP, IP and GP on Ω–μ plane. (b) and (c) Schematic diagrams for the geometry patterns of MPB, IP beam (IPB) and γ-ray beam (GB) on pole 1 and pole 2, respectively. Only parts of the MPB and GB are visible so that the LOS (the lower white line) does not cross these beams on P2, otherwise additional pulses would be produced. The emission beam is assumed to be approximately symmetric about the Ω–μ plane. Here, shown on the celestial sphere are only the original beams, the additional phase shifts caused by aberration, retardation and MSB effects are not presented.

Besides, Biggs (1990) performed an independent investigation of the MP/IP correlation and mode changing in PSR B1055−52 by studying the individual pulses. Their results also support the nature of two-pole origin of the radio pulses.

The uncertainty of the values of α and ζ does not change the basic conclusion either. van Ommen et al. (1997) obtained $\alpha = 78 \pm 5^\circ$ and $\zeta \simeq 112^\circ$ by fitting the PA curves at 950 MHz, which is slightly different from those given by LM88 at 640 MHz. When using $\alpha = 78^\circ$ and $\zeta = 112^\circ$, the constrained emission heights are less than those listed in Table 1 by about 10–20 per cent.

The measurements of radio and GP widths are different in this paper. Because the time resolution of γ-ray light curve is limited, the GP width is represented by the peak-to-peak separation, but not 20 per cent width as is chosen for radio pulse widths. If one chooses a consistent way to measure both radio and GP widths, the results will change slightly. For instance, if peak-to-peak phase separations are measured for radio MP and IP, the results of φ and r for components 'MP-L' and 'IP-L' will decrease a little compared with the present ones. Meanwhile, the results for other components may decrease or increase a little depending on how the MP centre (used as zero phase reference) is changed. However, these changes are not significant for B1055−52 because the profiles of radio MP and IP are roughly symmetrically shaped, so they do not change the basic conclusions.

As suggested by some authors (e.g. Blaskiewicz et al. 1991), the centre of the PA curve may be shifted with respect to the centre of the pulse profile due to aberration, retardation and MSB effects. For B1055−52, such phase lags are $\Delta\Phi_{\rm lag} = 0.^\circ5 \pm 2^\circ$ for the radio MP and $\Delta\Phi_{\rm lag} = 12^\circ \pm 2^\circ$ for the IP (measured from LM88's fig. 8). The 20 per cent peak-intensity pulse widths are used to determine the centres of profiles. The errors are due to measuring and time-sampling accuracy of the profile. The results in Table 1 can reproduce such phase lags naturally because at the beginning the longitudes of radio central emission positions are defined as those of the centres of PA curves and the longitudes of leading emission positions are designated as those of the leading edges (20 per cent peak intensity) at pulse profiles, meanwhile 20 per cent pulse widths are fitted to determine the leading positions, thus the phase lags have been involved in the constraining process. It should be noted that $\Delta\Phi_{\rm lag} = 12^\circ$ for the IP is only applicable to the case that no component is missing. The results of r for this case (IP-C‡ and IP-L‡) show that at least a difference of $0.1r_{\rm c}$ between the heights of leading and central positions is needed to generate the phase offset.

Comparing with the current high-energy models, the conventional polar cap model, which suggests that the γ-ray emission altitudes are about several times of the stellar radius, is not favoured. In the thick outer gap model, the thickness of the outer gap is estimated to occupy 0.74 times the outer magnetosphere of B1055−52 (Zhang & Cheng 1997), equivalently the inner boundary of the outer gap as well as the γ-ray emission region locates near the open field line with $\eta \simeq 0.7$. Meanwhile, the emission altitudes are suggested to be beyond the null charge surface. Therefore, the thick outer gap model is favoured. In the annular gap model, the γ-rays are suggested to be emitted near the central open field lines of the outer magnetosphere and near the null charge surface, thus this model is generally supported by our results.

ACKNOWLEDGMENTS

We are grateful to K. J. Lee and Dr J. H. Fan for their helpful discussion. We also appreciate the anonymous referee for his/her valuable comments. This work is supported by NSF of China (10403001, 10373002 and 10273001).

REFERENCES

Biggs J. D., 1990, MNRAS, 246, 341
Blaskiewicz M., Cordes J. M., Wasserman I., 1991, ApJ, 370, 643
Cheng K. S., Ho C., Ruderman M. A., 1986a, ApJ, 300, 500
Cheng K. S., Ho C., Ruderman M. A., 1986b, ApJ, 300, 522
Cheng K. S., Ruderman M. A., Zhang L., 2000, ApJ, 537, 964
Cordes J. M., 1978, ApJ, 222, 1006
Daugherty J. K., Harding A. K., 1996, ApJ, 458, 278
Dyks J., Rudak B., 2003, ApJ, 598, 1201
Fierro J. M. et al., 1993, ApJ, 413, L27
Gil J., Gronkowski P., Rudnicki W., 1984, A&A, 132, 312
Goldreich P., Julian W. H., 1969, ApJ, 157, 869
Harding A. K., 1981, ApJ, 245, 267
Hibschman J. A., Arons J., 2001, ApJ, 546, 382
Lyne A. G., Manchester R. N., 1988, MNRAS, 234, 477 (LM88)
McCulloch P. M., Hamilton P. A., Ables F. G., Komesaroff M. M., 1976, MNRAS, 175, 71
Muslimov A. G., Harding A. K., 2004, ApJ, 606, 1143
Phillips J. A., 1992, ApJ, 385, 282
Qiao G. J., Lee K. J., Wang H. G., Xu R. X., Han J. L., 2004, ApJ, 606, L49
Radhakrishnan V., Cooke D. J., 1969, Astrophys. Lett., 3, 225 (RC69)
Rankin J. M., 1993, ApJS, 85, 145
Shitov Y. P., 1983, Sov. Astron., 27, 314
Smirnova T. V., Shishov V. I., 1989, Pis'ma Astron. Zh., 15, 443
Thompson D. J. et al., 1999, ApJ, 516, 297
van Ommen T. D., Alessandro F. D., Hamilton P. A., McCulloch P. M. 1997, MNRAS, 287, 307

Wu X. J., Huang Z. K., Xu X. B., 2002, Chin. J. Astron. Astrophys., 2, 454
Zhang L., Cheng K. S., 1997, ApJ, 487, 370

APPENDIX A: GEOMETRICAL RELATIONS OF ϑ' AND δ

The angle ϑ' can be figured out from $\cos\vartheta' = \hat{k}\cdot\hat{v}$, where $\hat{v}$ and $\hat{k}$ are unit vectors of corotation velocity and photon direction in the corotation frame, respectively (see Fig. A1). Because in the corotation frame, photons are emitted along the direction of magnetic field, then we have $\cos\vartheta' = \hat{b}\cdot\hat{v}$, where $\hat{b}$ is the unit vector of magnetic field.

It is convenient to express the above unit vectors in the Cartesian coordinate system *oxyz*, of which the origin locates on stellar centre, $o\hat{z}$ is parallel to the rotation axis and $o\hat{x}$ lies on Ω–μ plane. An auxiliary Cartesian coordinate system is $ox'y'z'$ system, of which $o\hat{z}'$ is parallel to magnetic axis and $o\hat{x}'$ also lies on Ω–μ plane. Then, the angle between the x axes of these two systems is α.

For any emission position with unit radius vector $\hat{r}$, $\hat{v}$ can be written as $\{-\sin\phi, \cos\phi, 0\}$ in *oxyz* system, where ϕ is the azimuthal angle of $\hat{r}$. To obtain ϕ, we first express $\hat{r}$ in $ox'y'z'$ system as $\{\sin\theta\cos\varphi, \sin\theta\sin\varphi, \cos\theta\}$, and then transform it into *oxyz* system by using the following transform equations between the two coordinate systems

$$\begin{aligned} x &= x'\cos\alpha + z'\sin\alpha,\\ y &= y',\\ z &= -x'\sin\alpha + z'\cos\alpha. \end{aligned} \tag{A1}$$

We have three Cartesian components $\{x, y, z\} = \{\sin\theta\cos\varphi\cos\alpha + \cos\theta\sin\alpha, \sin\theta\sin\varphi, -\sin\theta\cos\varphi\sin\alpha + \cos\alpha\cos\theta\}$. Then, there is

$$\tan\phi = \frac{y}{x} = \frac{\sin\theta\sin\varphi}{\sin\theta\sin\varphi\cos\alpha + \cos\theta\sin\alpha}. \tag{A2}$$

Following the same procedure, the unit vector $\hat{b}$ at the emission position can be written as $\{\sin\theta_\mu\cos\varphi\cos\alpha + \cos\theta_\mu\sin\alpha, \sin\theta_\mu\sin\varphi, -\sin\theta_\mu\cos\varphi\sin\alpha + \cos\alpha\cos\theta_\mu\}$. Finally, we have

$$\begin{aligned} \cos\vartheta' &= \hat{b}\cdot\hat{v}\\ &= -\sin\phi(\sin\theta_\mu\cos\varphi\cos\alpha + \cos\theta_\mu\sin\alpha)\\ &\quad + \cos\phi\sin\theta_\mu\sin\varphi. \end{aligned} \tag{A3}$$

As to angle δ, it can easily be derived from the third Cartesian component of unit vector $\hat{r}$ in *oxyz* system, which reads

$$\cos\delta = -\sin\theta\cos\varphi\sin\alpha + \cos\alpha\cos\theta. \tag{A4}$$

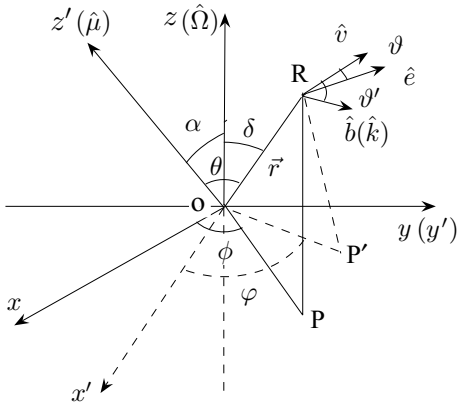

Figure A1. Coordinate systems and geometrical parameters. For an emission point 'R', $\vec{r}$ is the vector radius from stellar centre 'O' to 'R'. Points 'P' and 'P′' are the projections of 'R' on the *xy* (equator plane) and $x'y'$ planes. The original emission direction $\hat{k}$ is shifted to $\hat{e}$ due to aberration effect. See the text, for the definition of each parameter.

This paper has been typeset from a TEX/LATEX file prepared by the author.